Assimilation of *Megha-Tropiques* SAPHIR Observations in the NOAA Global Model

ERIN E. JONES AND KEVIN GARRETT

Riverside Technology, Inc., and NOAA/NESDIS/STAR, College Park, Maryland

SID-AHMED BOUKABARA

NOAA/NESDIS/STAR, College Park, Maryland

(Manuscript received 14 April 2016, in final form 10 June 2017)

ABSTRACT

The National Oceanic and Atmospheric Administration (NOAA) Global Data Assimilation System/Global Forecast System (GDAS/GFS) was extended to assimilate brightness temperatures from the Sondeur Atmosphérique du Profil d'Humidité Intertropicale par Radiométrie (SAPHIR) passive microwave water vapor sounder on board the *Megha-Tropiques* satellite. Quality control procedures were developed to assess the SAPHIR data quality for assimilating clear-sky observations over ocean surfaces, and to characterize observation biases and errors. A 6-week impact experiment was performed using the GDAS/GFS data assimilation system. The addition of SAPHIR observations on top of the current global observing system improved analysis and forecast humidity root-mean-square error (RMSE) results at the upper levels of the troposphere by about 6%, mostly at 100 hPa, when verified against European Centre for Medium-Range Weather Forecasts (ECMWF) analysis, though some degradation to the forecast humidity was seen at 150–200 hPa. The forecast impacts were predominant at earlier lead times between 24 and 96 h. Verification using global radiosonde observations also showed a reduction of the humidity RMSE from 4% to 6% between 500 hPa and the surface when assimilating SAPHIR, while temperature and wind speed RMSEs were reduced by up to 9% and 7% near the tropical tropopause, respectively. Other conventional forecast skill parameters including the 500-hPa geopotential height anomaly correlation showed neutral impact when assimilating SAPHIR.

1. Introduction

Water vapor is arguably one of the most important constituents of the atmosphere. Apart from being a potent greenhouse gas, water vapor is a key component of the hydrological cycle, and latent heat release from the condensation of water vapor plays a major role in the development of weather systems. An accurate knowledge of the distribution of water vapor throughout the atmosphere is therefore important to producing good weather forecasts. Accurately measuring atmospheric water vapor, however, can prove to be a challenge. Though radiosondes provide good information about the vertical distribution of moisture in the atmosphere, radiosonde networks offer sparse spatial and temporal sampling, especially over the ocean. Other ground-based remote sensing platforms (e.g., lidar and microwave profilers) provide useful data, but in relatively few locations over land. Satellite-based remote sensing allows for near-global coverage of measurements, albeit typically at lower spatial resolutions than some ground-based platforms, from which moisture information may be retrieved with high temporal sampling, making spaceborne platforms a valuable source of data for numerical weather prediction (NWP).

Spaceborne atmospheric measurements of water vapor typically come from infrared (IR) or passive microwave sensors. Atmospheric moisture is not measured directly from these instruments, but is rather retrieved from IR or microwave radiances or brightness temperatures. The methods of deducing water vapor amounts or distributions from satellite data are not fool proof; narrowband IR sensors, for instance, have limited vertical resolution and IR retrievals of water vapor in general are not effective in cloudy conditions (Seemann et al. 2003). Although passive microwave radiometers also have low vertical resolution, their signal is sensitive in most weather conditions, including in precipitation

Corresponding author: Erin E. Jones, erin.jones@noaa.gov

DOI: 10.1175/MWR-D-16-0148.1

TABLE 1. SAPHIR instrument channels, frequency, polarization, nominal noise equivalent differential temperature (NEDT), and bandwidth.

Channel	Frequency (GHz)	Polarization	NEDT (K)	Bandwidth (MHz)
1	183.31 ± 0.20	H	2.35	200
2	138.31 ± 1.10	H	1.45	350
3	183.31 ± 2.80	H	1.36	500
4	183.31 ± 4.20	H	1.38	700
5	183.31 ± 6.80	H	1.03	1200
6	183.31 ± 11.0	H	1.10	200

over ocean surfaces, to (depending on the sensor) total column water vapor (TPW) or atmospheric humidity profiles from the surface throughout the troposphere (Boukabara et al. 2010; Sun 1993).

Historically, it is the temperature information from microwave radiances that has typically been assimilated into NWP systems and has shown positive impact on medium-range weather forecasts, especially from the National Oceanic and Atmospheric Administration (NOAA) Polar-Orbiting Operational Environmental Satellite (POES) (e.g., *NOAA-18* and *NOAA-19*) and European Organisation for the Exploitation of Meteorological Satellites (EUMESAT) Meteorological Operational (MetOp) series satellites with Advanced Microwave Sounding Unit (AMSU-A) temperature sounders (English et al. 2000; McNally et al. 2000). Water vapor profile information is also available from the Microwave Humidity Sounder (MHS) on board these platforms, as well as from the Advanced Technology Microwave Sounder (ATMS) on board the *Suomi National Polar-Orbiting Partnership* (*SNPP*) satellite, and from the Special Sensor Microwave Imager/Sounder on the Defense Meteorological Satellite Program (DMSP) *F16–F19* series satellites, but impacts on NWP forecasts have, until recently, been mixed (Bengtsson and Hodges 2005). Much of the recent progress on the assimilation of microwave humidity sounding channels has shown positive impact on the

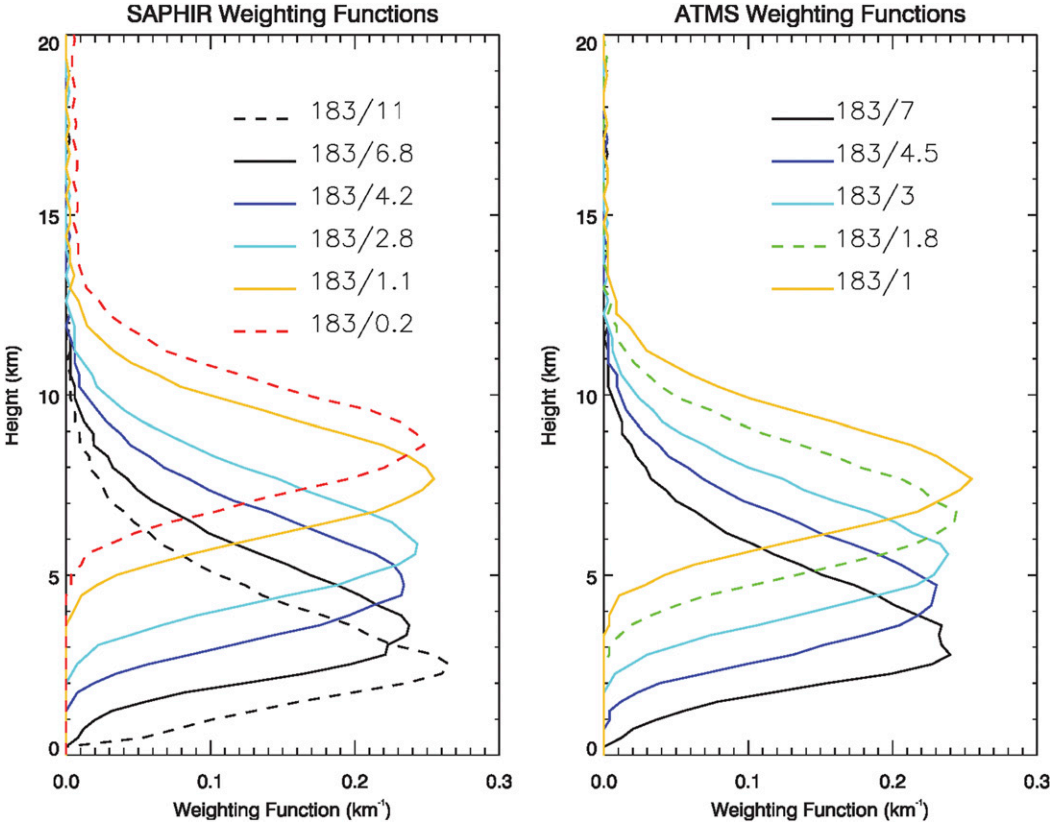

FIG. 1. Weighting functions for the 183-GHz channels of (left) SAPHIR and (right) ATMS.

TABLE 2. Regression coefficients for retrieving GWP from SAPHIR brightness temperature observations.

Angle bin ($x°$)	Constant (a_0)	Regression coefficients (b_x)
0–10	4.041 66	−0.000 85, −0.009 38, 0.045 94, −0.053 11, 0.003 45, −0.001 10
10–20	3.861 60	−0.004 78, −0.003 88, 0.066 88, −0.111 37, 0.062 39, −0.023 63
20–30	3.371 89	0.000 41, −0.014 16, 0.087 50, −0.138 36, 0.081 19, −0.029 05
30–40	2.330 67	0.003 44, −0.014 20, 0.089 30, −0.148 20, 0.095 56, −0.034 18
40–50	1.951 02	0.009 13, −0.025 69, 0.112 45, −0.176 90, 0.113 69, −0.039 43

analysis fields of water vapor, on temperature forecasts through correlations prescribed in background errors, and on wind forecasts through the use of water vapor fields as tracers (Andersson et al. 2007; Geer et al. 2014).

In this study, we focus on the assimilation of humidity observations from the Sondeur Atmosphérique du Profil d'Humidité Intertropicale par Radiométrie (SAPHIR) on board the *Megha-Tropiques* satellite, which measures radiances across six channels in the 183-GHz band and allows for the retrieval of atmospheric water vapor profiles over a greater vertical range of the atmospheric column compared to other microwave humidity sounders. Efforts to directly assimilate SAPHIR brightness temperatures in global and regional models have shown positive impacts on NWP forecasts (Chambon et al. 2015; Singh et al. 2013); considering the encouraging results of assimilating SAPHIR in the Météo-France global model, as presented in Chambon et al. (2015), we focus on assessing the impact of assimilation SAPHIR observations on the NOAA Global Data Assimilation System/Global Forecast System (GDAS/GFS). Section 2 provides a brief description of the SAPHIR instrument, data characteristics, and data assimilation quality control methodology. The impact of assimilating SAPHIR on both the analysis and forecast is presented in section 3, and a final summary is given in section 4.

2. SAPHIR description and data quality assessment

a. *SAPHIR sensor and data description*

The *Megha-Tropiques* satellite was launched on 12 October 2011 as a joint mission between the Indian Space Research Organization (ISRO) and the French

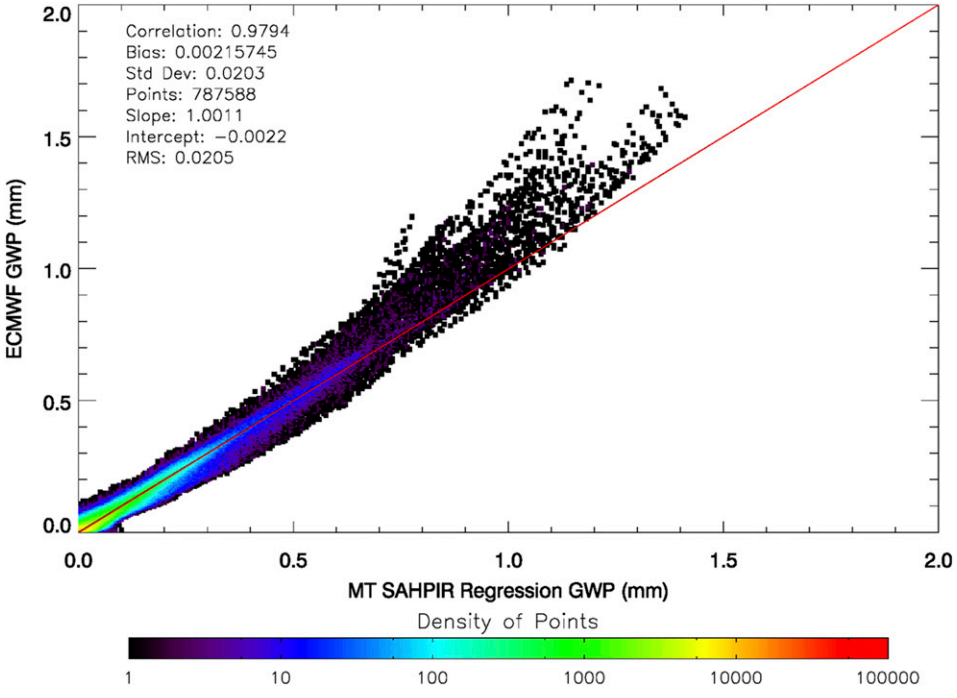

FIG. 2. Density scatterplot comparing derived GWP from simulated SAPHIR brightness temperatures to ECMWF cloud ice, for 1 day of simulated data.

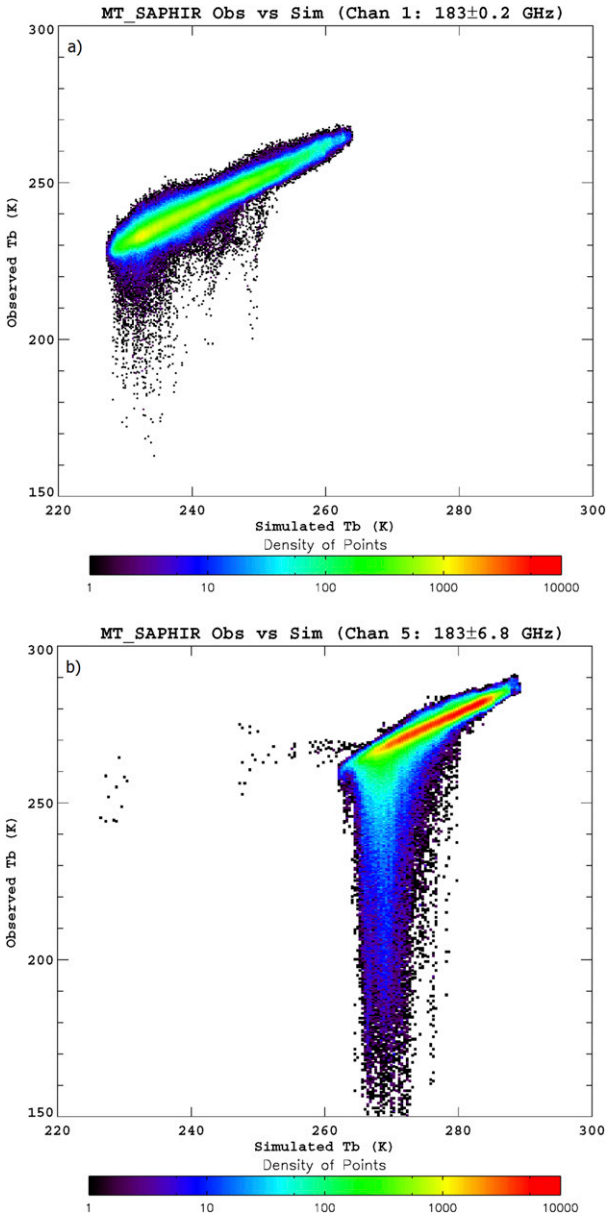

FIG. 3. Ocean-only observed vs simulated SAPHIR brightness temperatures for channels (a) 1 and (b) 5, for one cycle of data (0000 UTC 20 Sep 2014), with no filtering applied. Statistics for the full day are summarized in Table 3. SAPHIR brightness temperatures are simulated assuming clear-sky conditions.

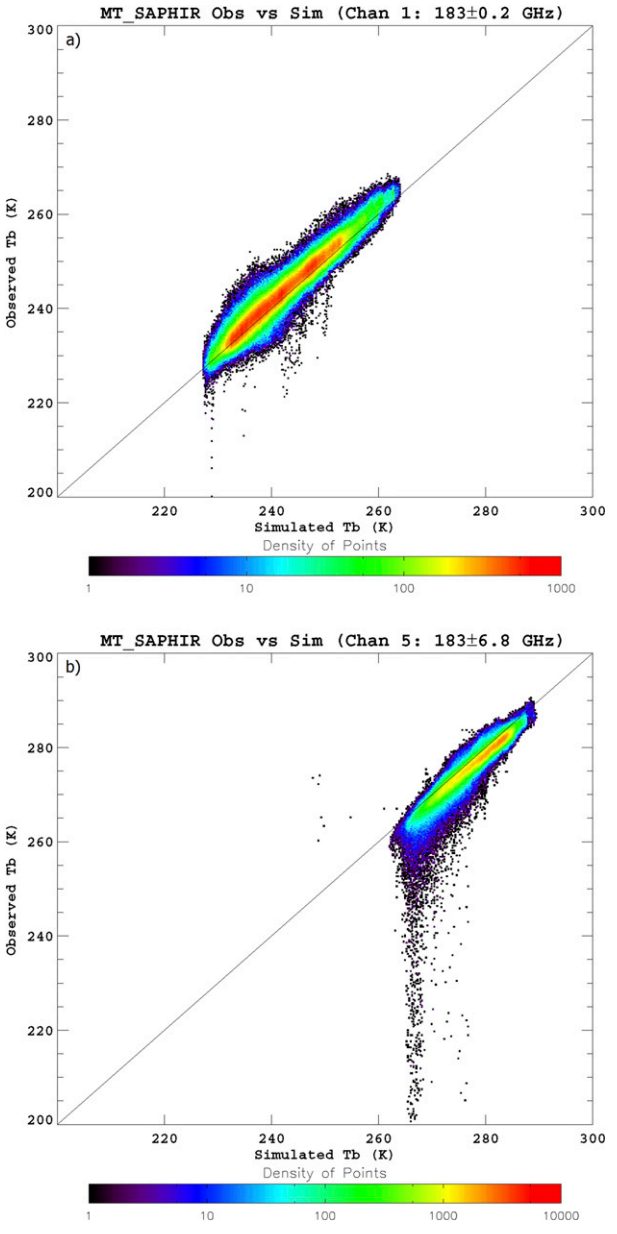

FIG. 4. As in Fig. 3, but after applying a GWP filter of 0.05 kg m^{-2}. Statistics for the full day are summarized in Table 3.

Centre National d'Etudes Spatiales (CNES). The satellite has a non-sun-synchronous orbit that is inclined at 20° with respect to the equator and provides ground coverage in the tropical latitudes from 22°S to 22°N. It houses the SAPHIR humidity sounder, which scans across track with a 1661-km swath width and 10-km horizontal resolution at nadir, and was designed specifically to serve as a passive microwave water vapor sounder, observing at six channels in the 183-GHz band (Table 1), which peak at different levels of the troposphere (Eymard et al. 2001). To illustrate the sensitivity of the SAPHIR channels to atmospheric water vapor, Fig. 1 shows the weighting functions for SAPHIR's channels in a standard tropical atmosphere. For comparison, Fig. 1 also shows the weighting functions for the 183-GHz channels on the *SNPP* ATMS sensor. Although the coverage is similar, it is clear that SAPHIR provides more vertical information of atmospheric water vapor, peaking about 1 km higher and 0.5 km lower in the troposphere than, respectively, the highest and lowest

TABLE 3. Statistical results from a preassimilation assessment of SAPHIR data quality. Results are for one day (20 Sep 2014) of comparing observed and simulated SAPHIR brightness temperatures, with and without filtering applied. Statistics are rounded to two decimal places.

		Unfiltered		Filtered	
Channel	Frequency (GHz)	Bias (K)	Std dev (K)	Bias (K)	Std dev (K)
1	183.31 ± 0.20	1.07	2.38	1.22	1.74
2	138.31 ± 1.10	−0.41	2.82	−0.11	1.40
3	183.31 ± 2.80	−1.45	4.49	−0.73	1.22
4	183.31 ± 4.20	−2.26	5.55	−1.26	1.11
5	183.31 ± 6.80	−2.59	7.02	−1.29	1.04
6	183.31 ± 11.0	−3.57	8.41	−1.93	0.96

weighting functions of ATMS. This is due to channels at 183 ± 0.2 and 183 ± 11 GHz, which peak higher and lower than any ATMS water vapor channels.

For the assimilation of SAPHIR brightness temperature observations, we use the SAPHIR L1A2 product. Though this study focuses only on demonstrating the impact of assimilating SAPHIR brightness temperatures into the GDAS/GFS, EUMETSAT began providing SAPHIR data in BUFR files to NOAA in near–real time in 2016, allowing for the possibility of operational assimilation of SAPHIR at the National Centers for Environmental Prediction (NCEP).

b. SAPHIR preassimilation data quality assessment

The focus of this work is on the assimilation of clear-sky SAPHIR brightness temperatures over ocean surfaces

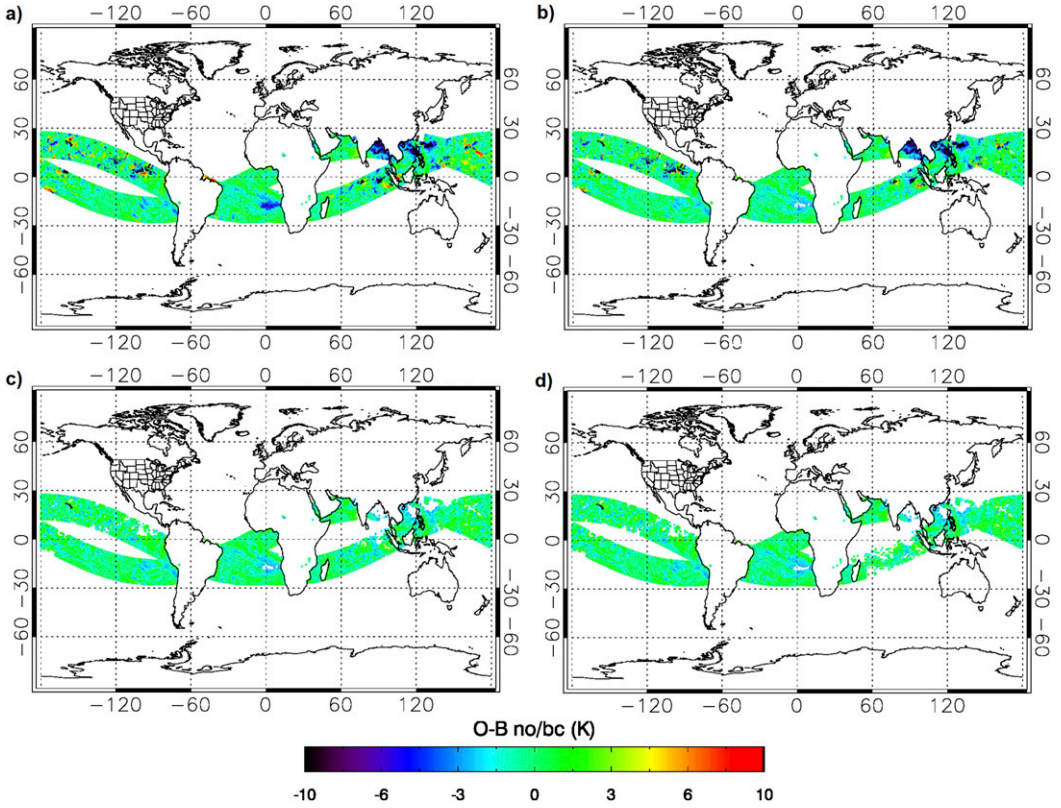

FIG. 5. The differences in observed and simulated SAPHIR brightness temperatures for channel 3 (183.31 ± 2.8H GHz) for 0000 and 0600 UTC cycles of the GSI on 17 Jul 2015 when (a) no filtering is applied, and when a gross check (3 K) and GWP filtering thresholded at (b) 0.07 kg m^{-2}, (c) 0.05 kg m^{-2}, and (d) 0.03 kg m^{-2}, are applied. As thresholds $<$ 0.05 kg m^{-2} do not appear to remove substantially more data points of high departure between the observed and simulated brightness temperatures, the 0.05 kg m^{-2} threshold was ultimately used in the experiments.

only. The preassimilation data quality assessment consists of comparisons of observed SAPHIR brightness temperatures with simulated observations to characterize biases, errors, and the effectiveness of quality control (QC) algorithms. The results of the assessment help to specify how the data are assimilated, including what observation errors (weights) to assign SAPHIR channels and how to implement QC procedures.

The 183-GHz water vapor sounding channels are mainly sensitive to atmospheric water vapor and to the scattering of convective cloud. The degree to which SAPHIR channels are sensitive to the scattering of ice cloud depends on the cloud-ice microphysical properties, the height of the cloud, and the channel frequency. For clear-sky assimilation, it is necessary to remove all observations affected by ice cloud, as these are not currently modeled adequately in the GDAS. To achieve this, a graupel water path (GWP) retrieval was developed for SAPHIR brightness temperatures. This retrieval is a multilinear regression trained on brightness temperatures that were simulated using the Community Radiative Transfer Model (CRTM; Han et al. 2006) and European Centre for Medium-Range Weather Forecasts (ECMWF) analysis of cloud ice as input. For training purposes, since the 183-GHz band is sensitive to cloud ice with large size distributions (typically effective radius $> 300\,\mu$m), the CRTM simulations assume an effective radius for cloud ice of 500 μm and ice density of 400 g m^{-3}. The retrieval uses all six SAPHIR channels to calculate GWP, and has distinct regression coefficients for each of five incidence angle bins (0°–10°, 10°–20°, 20°–30°, 30°–40°, and 40°–50°) to remove any scan dependence in the GWP retrieval. After selecting the correct bin for the incidence angle at the location of a set of SAPHIR brightness temperatures, the GWP is retrieved using the following formula:

$$\mathrm{GWP} = a_0 + \sum_{x=1}^{n} (\mathrm{TB}_x \times b_x),$$

where a_0 is a constant and TB_x and b_x are the brightness temperature and regression coefficient, respectively, specified at channel number x of n channels (in this case, $n = 6$). The regression coefficients and constants for each angle bin applied for the SAPHIR GWP retrieval are presented in Table 2. The retrieval results from the simulation are shown in Fig. 2, comparing the GWP derived from simulated SAPHIR brightness temperatures with the ECMWF cloud ice. The retrieval in the simulation shows very good agreement with ECMWF, especially for amounts below 0.7 mm, with a slight underestimation of GWP for values greater than 0.7 mm.

The preliminary data quality assessment with no filtering applied to SAPHIR observations is shown in Fig. 3. The scatterplots depict observed versus simulated SAPHIR brightness temperatures for 6 h (or one cycle) of data on 20 September 2014 for channels 1 (high peaking) and 5 (low peaking). The simulated brightness temperatures assume that the input ECMWF profiles are for clear sky. When spatially and temporally

TABLE 4. Operational sensors assimilated in the CNTRL and SAPHMT experiments. Here, *T*, *Q*, and *W* denote that temperature sounding, water vapor sounding, or window channels are assimilated, respectively.

Platform	Sensors assimilated	Channels
Aqua	AIRS	*T/Q*
	AMSU-A	
F17	SSMIS	*T*
F18	SSMIS	*T*
GOES-15	GOES Sounder	*T/Q*
Meteosat-10	SEVIRI	*T/Q*
MetOp-A	HIRS/4	*T/Q*
	AMSU-A	*T/W*
	MHS	*Q/W*
	IASI	*T/Q*
MetOp-B	AMSU-A	*T/W*
	MHS	*Q/W*
	IASI	*T/Q*
NOAA-15	AMSU-A	*T/W*
NOAA-18	AMSU-A	*T/W*
	MHS	*Q/W*
NOAA-19	AMSU-A	*T/W*
	MHS	*Q/W*
SNPP	ATMS	*T/Q/W*
	CRIS	*T/Q*

TABLE 5. Average statistics for SAPHIR OmB without bias correction (b/c) for all GDAS cycles between 7 Jun and 17 Jul 2015 with and without filtering.

		OmB (no filter, no b/c)			OmB (with filter, no b/c)		
Channel	Frequency (GHz)	Count ($\times 10^6$)	Bias (K)	Std dev (K)	Count ($\times 10^6$)	Bias (K)	Std dev (K)
1	183.31 ± 0.20	3.9	1.67	2.91	2.7	1.77	1.45
2	138.31 ± 1.10	3.9	0.34	3.23	2.8	0.45	1.37
3	183.31 ± 2.80	3.9	−0.18	4.59	2.9	−0.16	1.24
4	183.31 ± 4.20	3.9	−0.71	5.58	3.1	−0.75	1.18
5	183.31 ± 6.80	3.9	−0.79	7.04	3.1	−0.77	1.11
6	183.31 ± 11.0	3.9	−1.48	8.48	3.2	−1.47	1.01

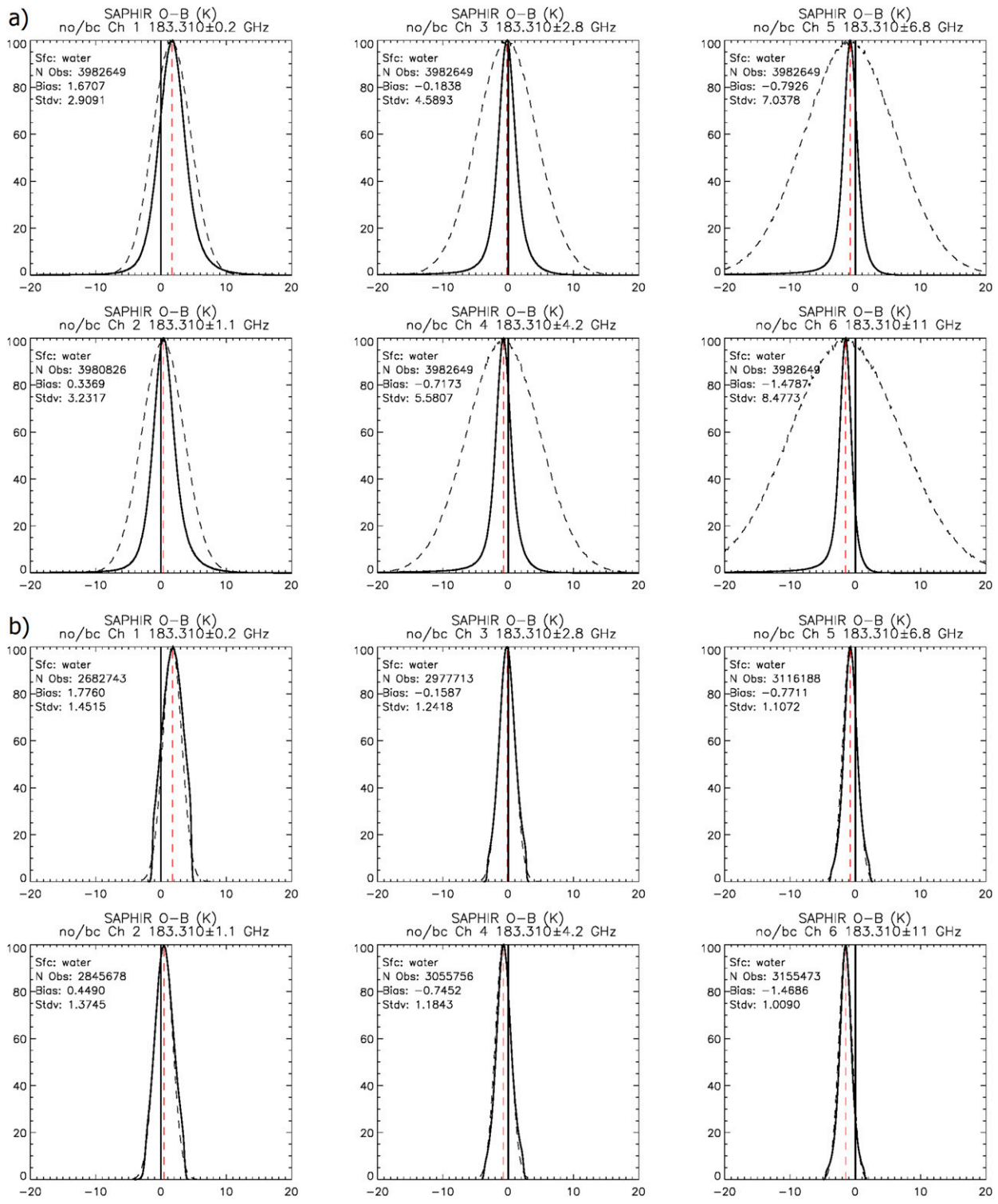

FIG. 6. Normalized OmB without bias correction for SAPHIR brightness temperatures from (top left to bottom right in each part) channels 1–6 for all cycles between 7 Jun and 17 Jul 2015 of the SAPHMT experiment when (a) quality control is not applied and (b) a GWP filtering of 0.05 kg m^{-2} is applied. Red dashed lines represent the mean bias determined by the peak of the histogram. Black dashed lines represent Gaussian distributions with the same means and standard deviations as the observed distributions.

collocated and compared with real brightness temperatures, the difference helps to illustrate which observations are affected by ice scattering, as the observations are much colder than the simulations in these instances. The degree of scattering is small for channel 1, the highest peaking water vapor channel, because of the saturation from water vapor absorption that occurs above the top of most ice clouds. For SAPHIR channel 5, which has further penetration depth into lower portions of the atmosphere, however, more scattering signature is apparent as a result of the presence of cloud: differences of upward of 60–80 K between observed and simulated brightness temperatures exist.

After applying the GWP regression to SAPHIR observations and removing points where retrieved GWP exceeds 0.05 kg m^{-2}, there is much better agreement between the observed and simulated brightness temperatures, as seen in Fig. 4. The large differences (colder observed brightness temperatures) seen in the unfiltered scatterplots are removed from the filtered scatterplots, and most of the remaining points fall along the one-to-one line, although a small portion of outliers remain. The statistical results for the observed minus simulated brightness temperatures (dTb) are summarized in Table 3 for both unfiltered and filtered data, for all SAPHIR channels. After filtering based on the GWP regression, the biases and standard deviations for all channels are reduced. The standard deviations are reduced from 2.38 to 1.74 K for the 183 ± 0.2 GHz channel, and from 8.41 to less than 1 K for the 183 ± 11 GHz channel. The reduction in error for the lowest peaking sounding channel of almost 7.5 K demonstrates the effectiveness of the GWP algorithm used for filtering. Figure 5 shows a map of the SAPHIR observed minus simulated brightness temperatures from channel 3 for unfiltered and filtered data from two cycles assimilating SAPHIR brightness temperatures in the GDAS with the GWP retrieval implemented for QC. After filtering the points affected by ice cloud, as determined by the GWP regression, the large brightness temperature depressions along the ITCZ are removed.

TABLE 6. As in Table 5, but for SAPHIR OmA with bias correction.

		OmA (with filter, with b/c)		
Channel	Frequency (GHz)	Count (×10^6)	Bias (K)	Std dev (K)
1	183.31 ± 0.20	3.1	−0.05	1.10
2	138.31 ± 1.10	3.2	−0.05	0.89
3	183.31 ± 2.80	3.2	−0.05	0.78
4	183.31 ± 4.20	3.2	−0.05	0.68
5	183.31 ± 6.80	3.2	−0.05	0.64
6	183.31 ± 11.0	3.2	0.00	0.62

3. SAPHIR analysis and forecast impacts

a. Methods

The SAPHIR observations are assimilated into the GDAS/GFS, which employs the Gridpoint Statistical Interpolation analysis system (GSI) scheme (Wang et al. 2013) for data assimilation. The GSI has the ability to ingest, QC, and assimilate satellite radiances from various platforms, as well as other types of observations like atmospheric motion vectors (AMVs), global positioning system radio occultation (GPSRO) observations, and conventional observations (e.g., radiosondes and aircraft data). It also includes error specifications for observations assimilated by the system, uses the CRTM for its forward and tangent linear calculations, and possesses a variational bias correction scheme for satellite radiances. The version of the GDAS/GFS used here employs CRTM version 2.1.3 and includes both hybrid 3DVar–ensemble Kalman filter (EnKF) and hybrid four-dimensional ensemble variational data assimilation (4DEnsVar) capabilities.

The retrieval and filtering techniques outlined in the previous section were implemented for QC of SAPHIR in the GSI, along with a gross check to remove any points where the departure of the observation from the background (OmB) for bias-corrected SAPHIR observations was greater than 3 K. The standard deviations presented in Table 3 that correspond to the filtered data have been used as the observation errors for SAPHIR in the data assimilation system. The biases shown in Table 3 are presented for informational purposes only; bias correction within the GDAS, as mentioned previously, is handled by the system's variational bias correction scheme (Zhu et al. 2014). For the assimilation and impact assessments in this study, we use the hybrid 3DVar–EnKF model, which runs an 80-member ensemble analysis and forecast for the generation of the ensemble portion of the background error covariance. Both the analysis and ensembles are run at T254/L64 resolution (about 50-km horizontal resolution with 64 vertical levels) and are cycled at four synoptic times (0000, 0600, 1200, and 1800 UTC). The GFS forecast, which uses a semi-Lagrangian dynamics scheme (McClung 2014), was run out to 168 h at a T670 resolution (about 25-km horizontal resolution) for the 0000 UTC cycle only. It should be noted that the resolutions used here for the GDAS analysis and GFS forecast are coarser than those that are employed in the operational GDAS/GFS.

Two experiments were run from 0000 UTC 1 June to 0000 UTC 18 July 2015 to assess the impact of assimilating SAPHIR observations. The first experiment

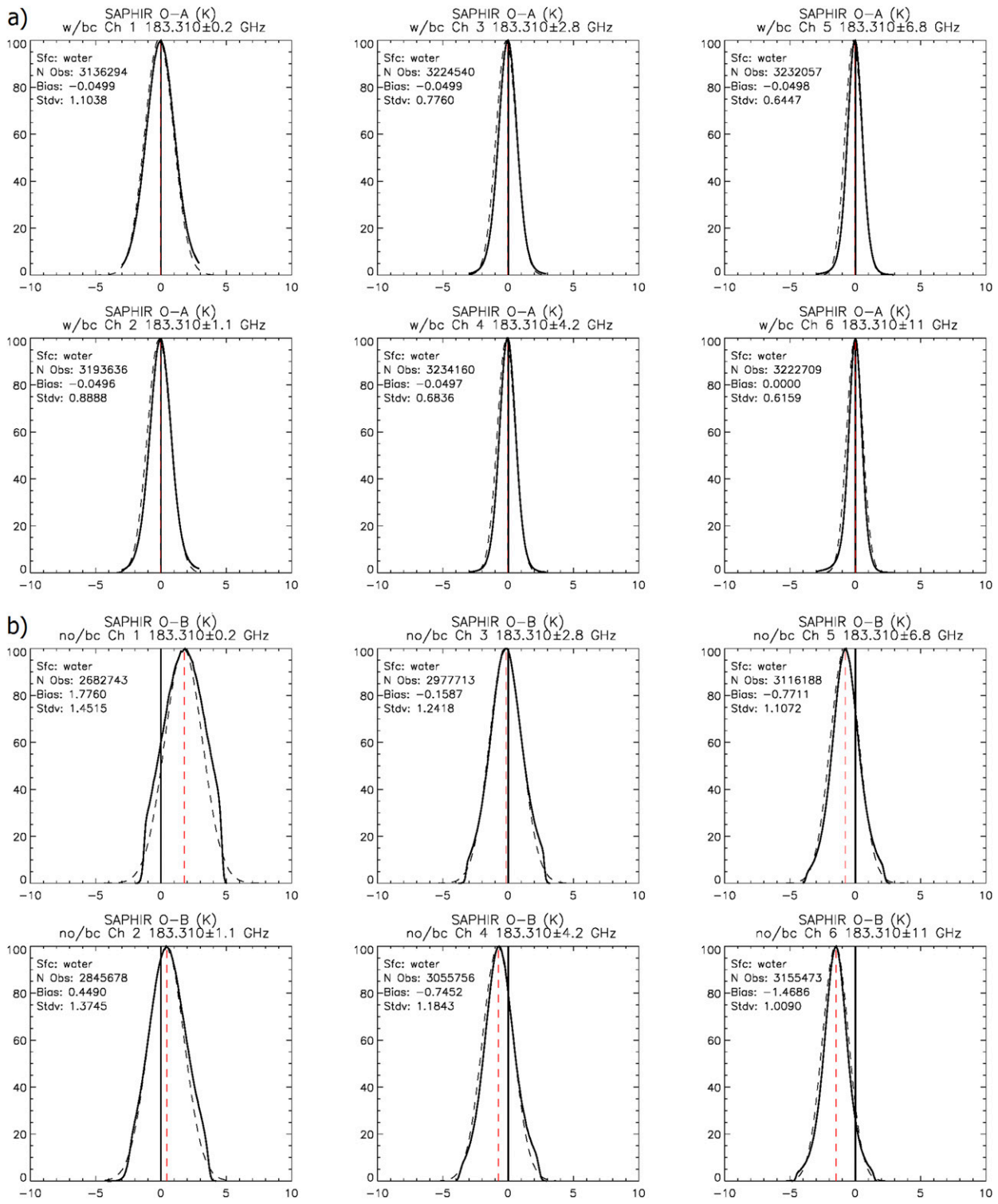

FIG. 7. As in Fig. 6, but for (a) OmA with bias correction for temperatures passing quality control; and (b) as in Fig. 6b, but with the *x*-axis scale reduced to −10 to 10.

TABLE 7. Statistical comparison of RH skill metrics over global and tropical regions for the CNTRL and SAPHMT analyses, when verified against ECMWF analyses. Results are averaged for 0000 UTC analyses over the time period 7 Jun–18 Jul 2015. Reductions in RMSE and standard deviation correspond to positive impacts in the SAPHMT analyses. Statistics are rounded to two decimal places, and changes are computed with respect to the CNTRL experiment. Statistics in bold are significant at the 95% confidence level.

	CNTRL		SAPHMT		Change with SAPHMT (%)	
Variable	RMSE	Std dev	RMSE	Std dev	RMSE	Std dev
Global RH 1000 hPa	7.34	5.28	7.29	5.25	**−0.68**	−0.57
Global RH 850 hPa	5.99	5.95	6.02	5.97	**+0.50**	+0.34
Global RH 700 hPa	4.22	4.16	4.22	4.17	0.00	+0.24
Global RH 500 hPa	3.07	2.95	3.08	2.95	+0.33	0.00
Global RH 300 hPa	5.55	3.69	5.47	3.65	**−1.44**	−1.08
Global RH 250 hPa	5.61	3.82	5.55	3.75	−1.07	−1.83
Global RH 200 hPa	4.47	4.24	4.51	4.23	**+0.89**	**−0.24**
Global RH 100 hPa	4.89	4.54	4.63	4.26	**−5.32**	**−6.17**
Tropical RH 1000 hPa	6.15	4.70	6.09	4.67	**−0.98**	−0.64
Tropical RH 850 hPa	5.09	5.00	5.30	5.16	**+4.13**	**+3.20**
Tropical RH 700 hPa	3.01	3.01	3.15	3.15	**+4.65**	**+4.65**
Tropical RH 500 hPa	3.11	3.05	3.14	3.04	+0.96	−0.33
Tropical RH 300 hPa	3.75	2.85	3.69	2.87	−1.60	+0.70
Tropical RH 250 hPa	5.35	3.46	5.34	3.44	−0.19	−0.58
Tropical RH 200 hPa	6.52	3.74	6.70	3.61	+2.76	**−3.48**
Tropical RH 100 hPa	7.08	6.66	6.66	6.15	**−5.93**	**−7.66**

(hereafter CNTRL) assimilated only those satellite observations used in the current (when the experiments were performed) operational GDAS/GFS (see Table 4). The second experiment (hereafter SAPHMT) was configured identically to CNTRL, but with SAPHIR data also assimilated. In addition to satellite radiances, both experiments also assimilated conventional observations from radiosondes, surface stations, buoys, and aircraft, as well as other satellite products including AMVs and GPSRO. The SAPHIR data were thinned to a 45-km grid, that is about the same size as the GDAS analysis grid, and assimilated for clear-sky, ocean-only cases, as previously mentioned. All other satellite radiance data were thinned onto a 145-km grid, as was standard in NCEP operations at the time the experiments were conducted. This choice of using a finer thinning grid for SAPHIR was made in an effort to take advantage of SAPHIR's higher spatial resolution when assimilating SAPHIR data. The first six full days of the experimental time period are taken as spinup, and are not used in the following assessments of analysis and forecast impacts.

A variety of methods were used to assess the impact of SAPHIR on the GDAS analysis and GFS forecast. ECMWF analysis fields were used as a reference to verify GDAS analyses and GFS forecasts from the CNTRL and SAPHMT experiments, with standard deviation and root-mean-square error (RMSE) used as the primary metrics of skill. Since SAPHIR is a water vapor sounder, assessment has mostly been focused on the analysis and forecast fields of relative humidity (RH), as well as on the analysis increments of RH, at varying vertical levels. The OmB statistics from other sensors with 183-GHz channels were also assessed to help quantify the impacts of assimilating observations from SAPHIR, as were comparisons to radiosonde observations.

b. SAPHIR impacts on the GDAS analysis

The first step in the post-assimilation assessment is to compare SAPHIR observations to simulated brightness temperatures based on both the background fields (OmB) and analysis fields (OmA). The results determine the effectiveness of the QC methods, bias correction schemes, and observation weights.

Results from the GSI when SAPHIR brightness temperatures are assimilated suggest that the QC scheme is effective at removing points where the forward model has difficulty simulating SAPHIR observations (e.g., in precipitating conditions) using the GWP regression for cloud screening. Table 5 shows the OmB without bias correction applied, for all six SAPHIR channels. The SAPHIR OmB standard deviation and bias values presented in Table 5 are of similar magnitude as those seen in Table 3 for a preassimilation assessment of the filtered and unfiltered data. Subtle differences can be noted, including larger positive biases at channels 1 and 2, and less negative biases for channels 3–6. These differences could be due to differences in the model profile input (ECMWF versus GDAS), or the filtering where GDAS also employs a gross error check. The

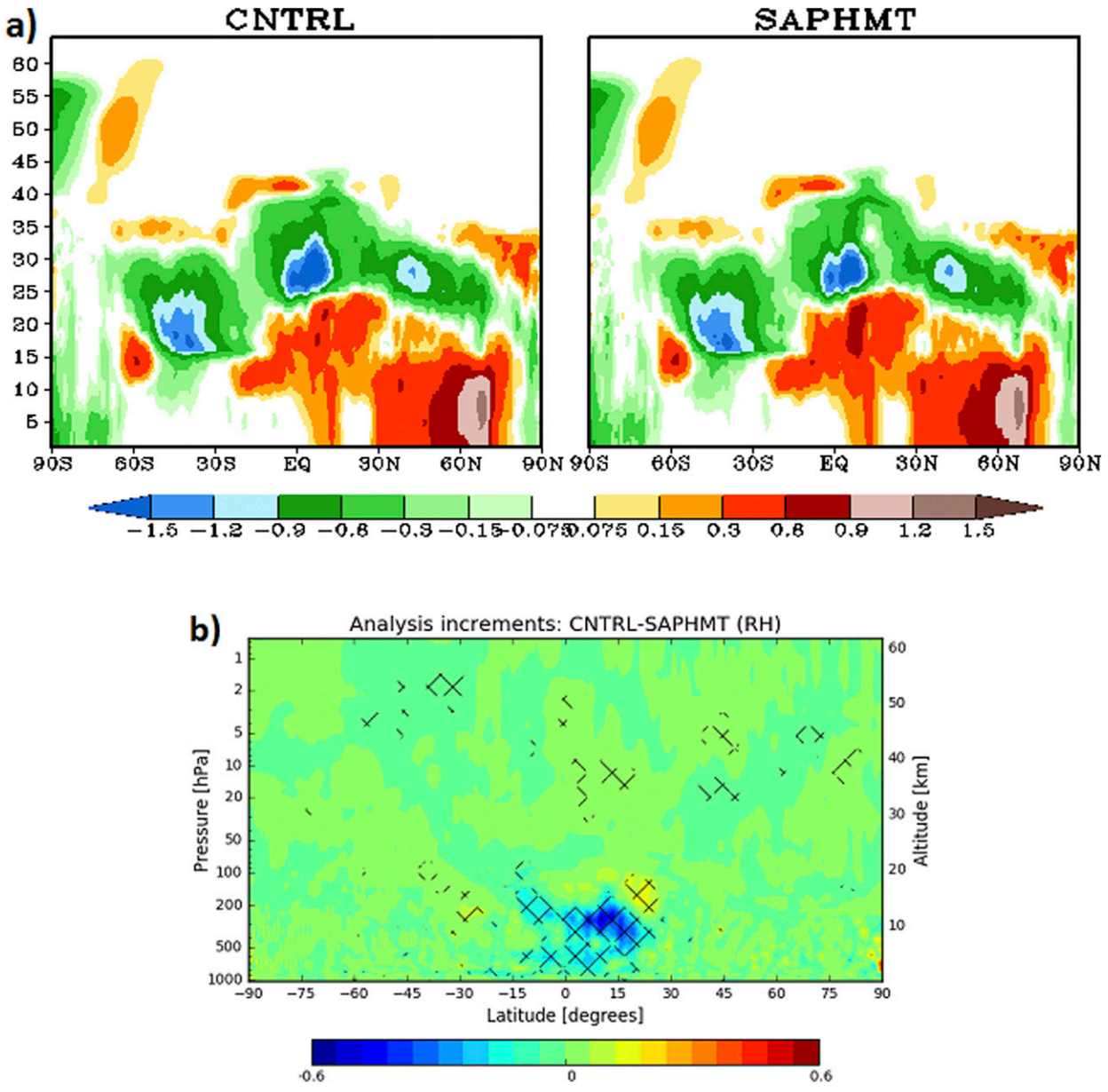

FIG. 8. (a) Vertical cross section (over all model levels: for reference, model level 1 is at the surface, model level 14 is ~850 hPa, model level 25 is ~520 hPa, and model level 41 is at ~100 hPa) of average RH analysis increments (%) for (left) CNTRL and (right) SAPHMT experiments, and (b) the difference in RH analysis increments between the CNTRL and SAPHMT experiments over the time period of 7 Jun–18 Jul 2015. In the difference plot, cooler colors (e.g., blue) indicate that RH increments are greater in the SAPHMT experiment, and hatching indicates RH analysis increment differences that are significantly different at the 95% confidence level. It should be noted that the vertical axes in (a) use model sigma levels, while the vertical axis in (b) uses approximate pressure levels on a log scale. The GDAS/GFS uses sigma levels and not constant pressure levels.

patterns in the SAPHIR OmB bias and standard deviation, however, are consistent with those seen in the preassimilation assessment results for both unfiltered and filtered data. When the data are filtered, the standard deviation decreases as the channels peak lower in the atmosphere. The bias for SAPHIR also is initially positive for channel 1, but decreases with channel number, becoming more negative as the channels peak closer to the surface. This pattern of the bias is consistent with other studies assessing the performance of the 183-GHz band from SAPHIR and other passive microwave humidity sounders with similar channels (Brogniez et al. 2016). Histograms, binned at 0.1 K and normalized by the maximum number of observations in a bin, show

TABLE 8. OmB standard deviation for 183-GHz channels from SSMIS *F17* and ATMS from CNTRL and SAPHMT experiments, averaged over the time period from 0000 UTC 7 Jun to 1800 UTC 5 Jul 2015. Statistics in bold indicate significant decreases in OmB standard deviation with the SAPHMT experiment at the 95% confidence level. SSMIS channels 9–11 are only monitored, not assimilated, in the experiments. ATMS channels 18–22 were assimilated in the experiments.

SSMIS *F17* Channel	Frequency	CNTRL Std dev	SAPHMT Std dev	Assimilated
9	183.31 ± 6.6 GHz	1.098	**1.064**	No
10	183.31 ± 3 GHz	1.183	**1.160**	No
11	183.31 ± 1 GHz	1.366	**1.342**	No
ATMS Channel	Frequency	CNTRL Std dev	SAPHMT Std dev	Assimilated
18	183.31 ± 7 GHz	0.877	**0.868**	Yes
19	183.31 ± 4.5 GHz	0.919	**0.911**	Yes
20	183.31 ± 3 GHz	0.963	0.956	Yes
21	183.31 ± 1.8 GHz	0.992	0.986	Yes
22	183.31 ± 1 GHz	1.048	1.044	Yes

results for OmB unfiltered (Fig. 6a) and OmB filtered (Fig. 6b) from all GDAS cycles between 7 June and 18 July 2015. The histograms in Fig. 6b show the impact of the quality control, clipping the tails and making the distributions more Gaussian compared to those in Fig. 6a.

Table 6 shows OmA statistics after bias correction, specifically the bias and standard deviation of the observations minus the simulated analysis fields after assimilating SAPHIR data. For all channels, there is a large reduction in standard deviation when compared to the OmB statistics, to below 1 K (close to 0.5 K) for channels 2–6. In fact, the residual standard deviations are well below the prescribed observation errors assigned from the preassimilation assessment results shown in Table 3, showing that the analysis fields are fitting the SAPHIR observations and the variational bias correction scheme is working for SAPHIR. Figure 7a shows the normalized histograms of OmA after bias correction, and the narrowing of the distribution compared to Fig. 7b, which shows again the OmB after filtering but with a restricted x axis from −10 to 10 K. The OmA histograms also show the removal of the radiometric bias.

The second part of the post-assimilation assessment investigates the impact that the assimilation of SAPHIR brightness temperatures has on the GDAS analysis geophysical fields, by comparing the analyses from the CNTRL and SAPHMT experiments to corresponding ECMWF analyses for reference and verification. Within this context, the nature (positive or negative) of an impact is determined by whether the analysis becomes more or less ECMWF like compared to CNTRL when SAPHIR is assimilated. As mentioned previously, the main impacts were expected to occur in moisture fields, and thus the RH at varying pressure levels was examined. Statistics (RMSE and standard deviation of the departure of the analysis from ECMWF) were computed for the CNTRL and SAPHMT experiments over the length of the experiment, and the results, summarized in Table 7, were subjected to a paired, two-tailed t test in order to determine whether they were significantly different at the 95% confidence level. Results indicate that, for most levels, SAPHIR has a neutral or slightly positive impact on the analyzed RH globally. The addition of SAPHIR has the largest impact on the analysis at 100 hPa, or about model level 41, where the reduction in RH RSME is around 5% globally when verified against ECMWF and compared to the CNTRL experiment. Improvements at other levels were generally more modest or neutral globally, excepting at 200 and 850 hPa, where some small, but significant, degradation in RMSE is seen. Results in the tropics are generally similar to those seen in the global domain; SAPHIR has a neutral or slightly positive impact on the analyzed RH for most levels. The impact is greatest at 100 hPa, where there was nearly a 6% reduction in RMSE when SAPHIR was assimilated and the results were verified against ECMWF. Results at other levels in the tropics were largely neutral, excepting at 700 and 850 hPa, where a significant degradation of 3%–5% is found in the standard deviation and RMSE scores when SAPHIR data are assimilated.

One possible explanation why SAPHIR would have the greatest impact (e.g., change with respect to the CNTRL experiment) on analysis RH at higher levels of the atmosphere is simply that it provides more humidity information in the upper troposphere compared to other passive microwave sounders. RH analysis increments averaged over the experiment time period show that SAPHIR is largely adding moisture information to the analysis at the mid- to upper levels in the tropics, as shown in Fig. 8 (not an unreasonable finding, since SAPHIR observations are limited to tropical latitudes). In general, it appears as if SAPHIR is adding more

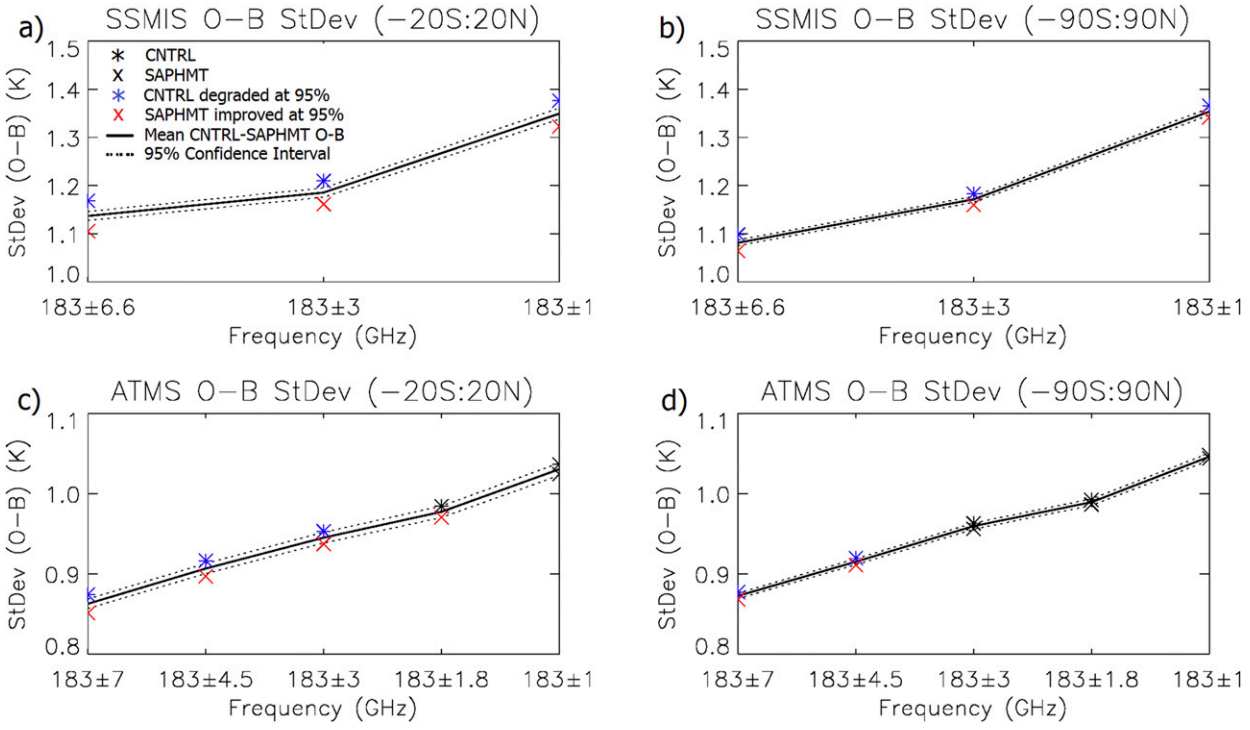

FIG. 9. Mean of the CNTRL (*) and SAPHMT (×) OmB standard deviation computed between 7 Jun and 17 Jul 2015 over the tropics and globally for (a),(b) SSMIS and (c),(d) ATMS water vapor channels. Dashed lines indicate the 95% confidence interval. Black symbols reflect that the standard deviations for the experiments are not significantly different. Blue (*) illustrates that the CNTRL OmB is significantly degraded without SAPHIR assimilated, while the red (×) illustrates that the SAPHMT OmB is significantly improved with SAPHIR assimilated.

moisture to the analysis (or taking away less moisture) than the CNTRL experiment at these latitudes. It also appears that many of these changes are significant at the 95% confidence level (see Fig. 8b; regions where RH analysis increments are significantly different between the CNTRL and SAPHMT experiments are hatched). Though a bulk of the information SAPHIR is adding to the analysis is occurring between 30°S and 30°N, SAPHMT RH analysis increments do differ slightly from CNTRL RH analysis increments in the midlatitudes and near the poles (especially in the Northern Hemisphere), though these changes are largely not significant.

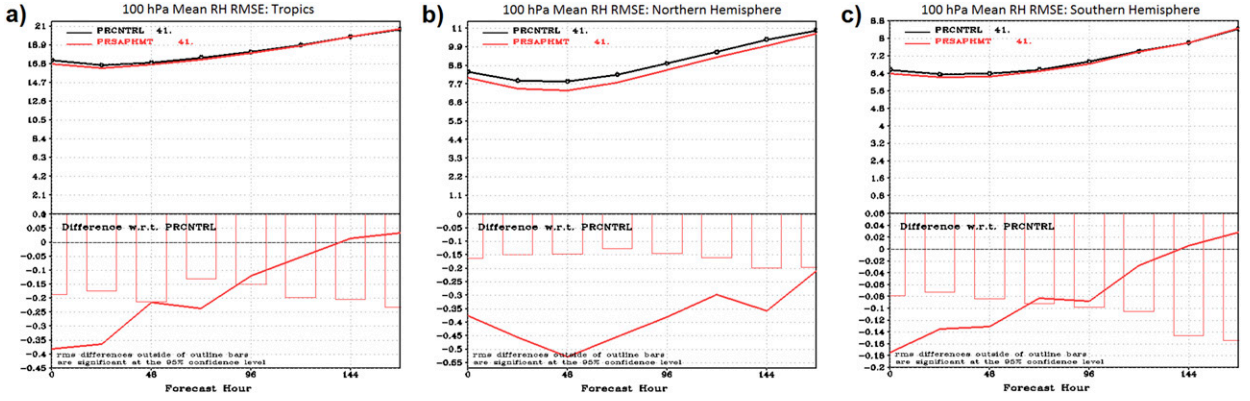

FIG. 10. Averaged 100-hPa RH RMSE (%) of day 1–7 forecasts from the CNTRL and SAPHMT experiments verified against ECMWF analyses for 0000 UTC forecasts over the time period of 7 Jun–18 Jul 2015. Results are shown for the RH RMSEs in the (a) tropics, (b) Northern Hemisphere (NH), and (c) Southern Hemisphere (SH). (top) The black line indicates the RMSE of the CNTRL and the red line indicates the RMSE of the SAPHMT experiment. (bottom) The corresponding RMSE differences of the SAPHMT experiment with respect to the CNTRL. The scores outside of the vertical bars in the bottom panel are statistically significant at the 95% confidence level.

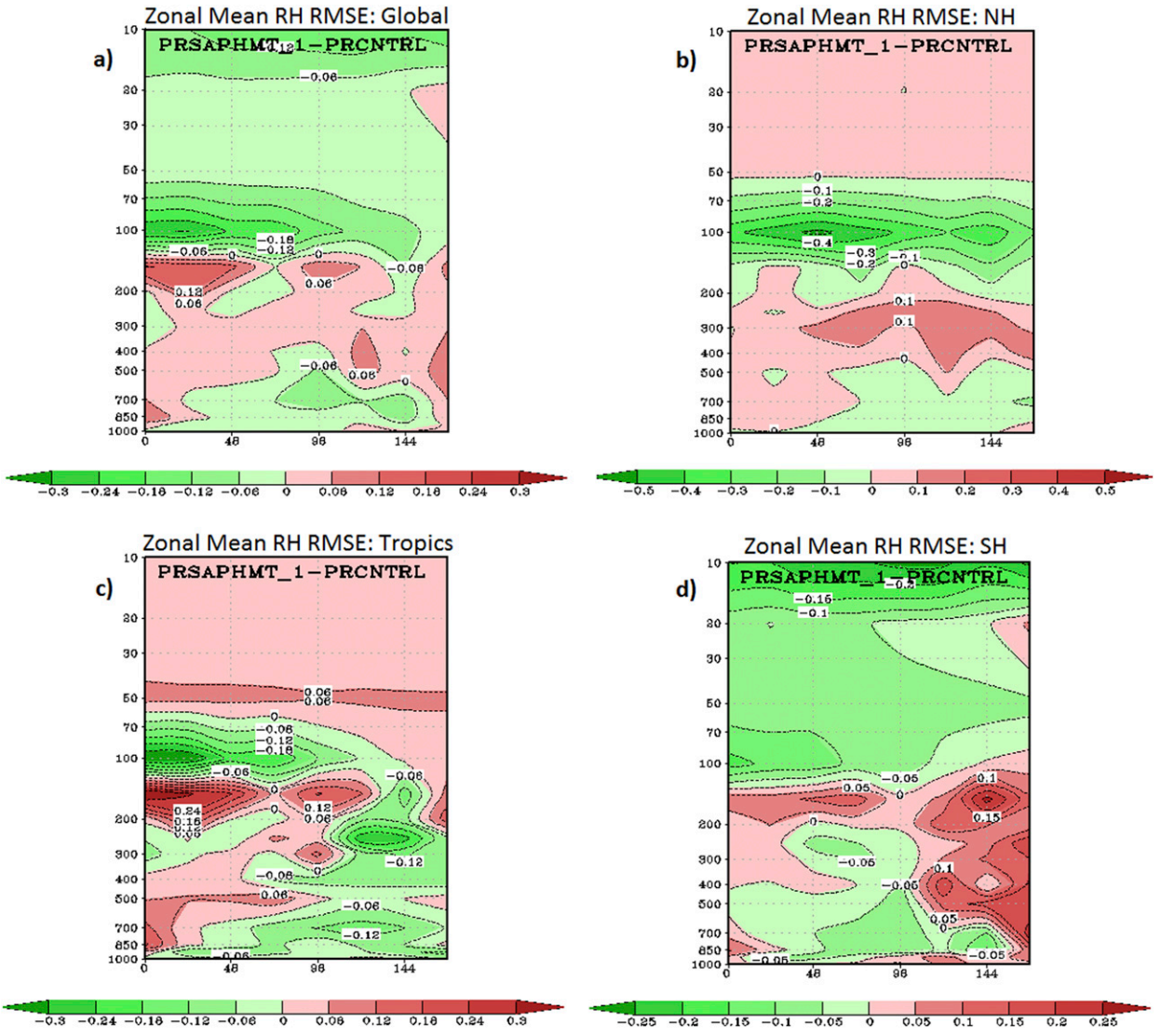

FIG. 11. Vertical cross sections (1000 to 10 hPa) of the zonal mean differences in forecast RH RMSE (%) between the SAPHMT and CNTRL experiments vs forecast time for (a) the global domain, (b) the NH, (c) the tropics, and (d) the SH. Results are averaged for 0000 UTC forecasts over the time period from 7 Jun to 18 Jul 2015. Green areas indicate regions of improvement in forecast RH in SAPHMT when verified against ECMWF, while red areas indicate regions of degradation in forecast RH.

The statistics for OmB without bias correction for other sensors with similar water vapor channels were also assessed between the CNTRL and SAPHMT experiments, to further gauge the impact of assimilating SAPHIR observations. Of interest were the 183-GHz channels from *SNPP* ATMS and *F17* SSMIS. All observations from both instruments were used to assess the global impact of assimilating SAPHIR, which is limited to observing tropical latitudes. Furthermore, to test the statistical significance of differences in CNTRL and SAPHMT OmB, a two-sample *t* test was performed on the mean of OmB standard deviations, where the populations of the standard deviation are given in each GDAS cycle. The results are summarized in Table 8. For both the SSMIS and ATMS 183-GHz channels, there is improvement to the OmB standard deviation when SAPHIR is assimilated. All SSMIS water vapor channels were significantly improved at the 95% confidence level, while only the lowest peaking ATMS channels had significant improvement (183 ± 7 and 183 ± 4.5 GHz). Figure 9 illustrates this result and compares the OmB for SSMIS and ATMS at tropical latitudes (Figs. 9a,c) to a globally computed OmB (Figs. 9b,d). The plots show the mean OmB between the CNTRL and SAPHMT experiments along with the 95% confidence intervals, as a function of channel frequency. The symbols represent

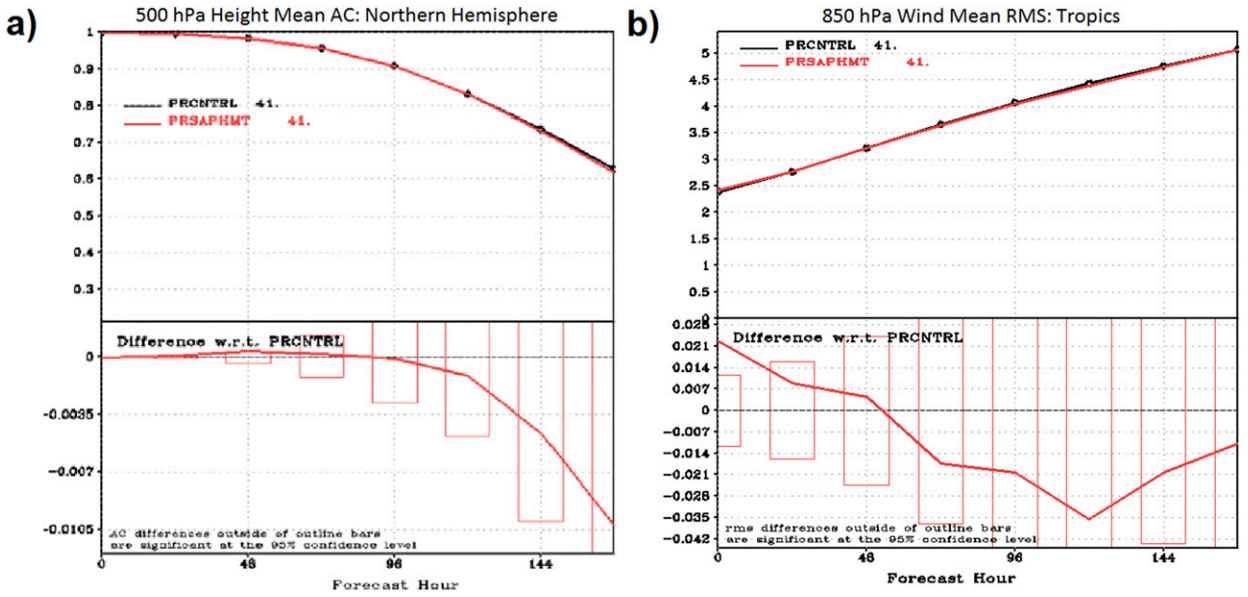

FIG. 12. (a) The averaged 500-hPa geopotential height AC of day 1–7 forecasts over the NH for the experimental period 7 Jun–18 Jul 2015 for CNTRL and SAPHMT experiments verified against the ECMWF analysis, and (b) 850-hPa wind speed RMSE ($m\,s^{-1}$) over the tropics. (top) The black line indicates the statistics of the CNTRL experiment and the red line indicates the statistics of the SAPHMT experiment. (bottom) The corresponding AC and RMSE differences of the SAPHMT experiment with respect to the CNTRL experiment. The scores outside of the vertical bars in the bottom panel are statistically significant at the 95% confidence level.

the OmB for each channel and each experiment, with blue indicating a statistically significant increase in OmB for CNTRL, and red indicating a statistically significant decrease in OmB when SAPHIR is assimilated into SAPHMT. As with the global scores, the addition of SAPHIR reduces the OmB significantly for SSMIS observations in the tropics. For ATMS, the analysis of OmB in the tropics shows more significant impact than for global observations, with four channels showing a significant reduction at the 95% confidence level. The overall improvement in the OmB statistics of SAPHIR-like channels for the other sensors suggests that SAPHIR is improving the background water vapor field (i.e., the short-term forecast) and therefore improving the background fit to the observations. It might be expected that adding SAPHIR water vapor information would have a larger impact in the tropics compared with the global fields, as illustrated in Fig. 9.

c. *SAPHIR impact on the GFS forecast*

To assess the impact that the assimilation of SAPHIR brightness temperatures has on the GFS forecast, forecasts from the CNTRL and SAPHMT experiments were verified at their valid times against corresponding ECMWF analyses, as well as against radiosonde observations. The focus was on assessing the impact that assimilating SAPHIR observations has on the forecast fields of RH, temperature, and wind, as well as on standard metrics used to determine global model forecast skill, such as the height anomaly correlation.

When verified against ECMWF analyses, the addition of SAPHIR brightness temperatures has a positive impact on forecast RH at upper levels, as is consistent with the analysis impacts described in the previous section. We show the RH RMSE at 100 hPa as a function of forecast time (Fig. 10, top) for the CNTRL and SAPHMT experiments, as well as the difference in RH RMSE with respect to the CNTRL (Fig. 10, bottom). For each region, including the tropics (Fig. 10a), Northern Hemisphere (Fig. 10b), and Southern Hemisphere (Fig. 10c), there is significant reduction in the 100-hPa RH RMSE up to around 0.5% RH for forecast times up to 72 h (though the impact is close to neutral in the tropics at 48 h). The 100-hPa RH RMSE continues to stay significantly lowered until 96 h in the tropics and through 168 h in the Northern Hemisphere.

Figure 11 shows the vertical cross sections of RH RMSE as a function of forecast hour for the global, Northern Hemisphere, Southern Hemisphere, and tropical domains. The reduction in forecast 100-hPa RH RMSE shown in Fig. 10 is evident for all regions examined out to 96 h. The largest significant positive impacts (as illustrated in Fig. 10) are in the Northern Hemisphere and tropics. A more modest, significant positive impact is seen in the Southern Hemisphere, which shows the improvement extending farther into

TABLE 9. Statistical results for 0000 UTC forecast AC and RMSE for select variables in the CNTRL and SAPHMT experiments, when verified against ECMWF analyses, over the time period from 7 Jun to 18 Jul 2015. Positive (negative) changes in AC scores indicate improvement (degradation) when SAPHIR is assimilated, and negative (positive) changes in RMSE scores indicate improvement (degradation) when SAPHIR is assimilated; significant changes are shown in boldface. Changes are computed with respect to the CNTRL experiment.

	CNTRL		SAPHMT		Change (%)	
	AC	RMSE	AC	RMSE	AC	RMSE
500-hPa height, day 5 NH	0.83	39.40	0.83	39.57	0.00	0.43
500 hPa height, day 5 SH	0.86	58.77	0.85	59.74	−1.16	+1.65
850-hPa temp, day 5 global	0.72	2.57	0.72	2.57	0.00	0.00
850-hPa winds, day 1 tropics	0.87	2.76	0.87	2.77	0.00	+0.36
850-hPa winds, day 3 tropics	0.77	3.66	0.77	3.64	0.00	−0.55
250/200-hPa winds, day 1 tropics	0.92	5.07	0.91	5.17	**−1.09**	**+1.97**
250/200-hPa winds, day 3 tropics	0.83	7.32	0.83	7.37	0.00	+0.68
1000-hPa RH, day 3 tropics	—	9.44	—	9.41	—	−0.32
1000-hPa RH, day 3 NH	—	13.80	—	13.79	—	−0.07
1000-hPa RH, day 3 SH	—	9.74	—	9.75	—	+0.10
850-hPa RH, day 3 tropics	—	15.58	—	15.49	—	−0.58
850-hPa RH, day 3 NH	—	16.79	—	16.77	—	−0.12
850-hPa RH, day 3 SH	—	22.51	—	22.43	—	−0.36
500-hPa RH, day 3 tropics	—	19.92	—	20.02	—	+0.50
500-hPa RH, day 3 NH	—	23.88	—	23.85	—	−0.13
500-hPa RH, day 3 SH	—	26.14	—	26.13	—	−0.04
150-hPa RH, day 1 tropics	—	20.55	—	20.86	—	**+1.51**
150-hPa RH, day 1 NH	—	10.89	—	10.91	—	+0.18
150-hPa RH, day 1 SH	—	7.32	—	7.40	—	+1.09
150-hPa RH, day 3 tropics	—	23.70	—	23.74	—	+0.17
150-hPa RH, day 3 NH	—	13.97	—	13.81	—	**−1.15**
150-hPa RH, day 3 SH	—	9.04	—	9.16	—	+1.33
100-hPa RH, day 3 tropics	—	17.48	—	17.24	—	**−1.37**
100-hPa RH, day 3 NH	—	8.26	—	7.80	—	**−5.57**
100-hPa RH, day 3 SH	—	6.58	—	6.49	—	−1.37

upper levels (e.g., to 50 hPa and above), whereas impacts at these levels were found to be neutral or negative in other regions of the globe (significance metrics not shown here).

The impact throughout the column below 100 hPa is mostly statistically neutral for RH in different regions of the globe. Over the tropics, the change in RH RMSE is mostly neutral below 100 hPa out to day 7, with some significant improvement seen at 700 hPa on days 4–5 and at 1000 hPa on day 7, and some significant degradation at 150–200 hPa on day 1–2, which appears to be related to similar degradations seen for certain cycles in time series of forecast skill scores for wind and temperature in the tropics around these levels (not shown). Investigations of forecast and analysis fields, as well as OmB and OmA residuals, have not identified the root cause of the degradations found during these isolated time periods. In the Southern Hemisphere, the impact of assimilating SAPHIR on forecast RH RMSE is neutral below 100 hPa, as is the impact in the Northern Hemisphere, although there are some levels that show increased RH RMSE (not significant). Overall, the impact of assimilating SAPHIR on the GFS forecast is consistent with the impact on the analysis. The largest forecast impacts from SAPHIR assimilation are on the RH at 100 hPa. The impact of assimilating SAPHIR observations on RH forecasts at mid- and lower levels in the atmosphere is found to be more modest or neutral.

To ensure that the assimilation of SAPHIR data was not negatively impacting non-RH variables, forecast fields of winds, temperature, and geopotential height were also verified against ECMWF analyses. We show the 500-hPa geopotential height anomaly correlation (AC) for the Northern Hemisphere as a function of forecast hour for the CNTRL and SAPHMT experiments (Fig. 12a), as well as the 850-hPa wind speed RMSE as a function of forecast hour over the tropics (Fig. 12b). The bottom panels of the plots demonstrate the difference between the AC and RMSE scores. In each case, the differences in the SAPHMT forecast from the CNTRL forecast are not beyond the 95% significance level, as defined by the boxed areas. Table 9 provides a summary of the results for all parameters at various levels and over regions. As assessed previously, the most significant impacts are seen in improvement in the upper-tropospheric RH forecast fields.

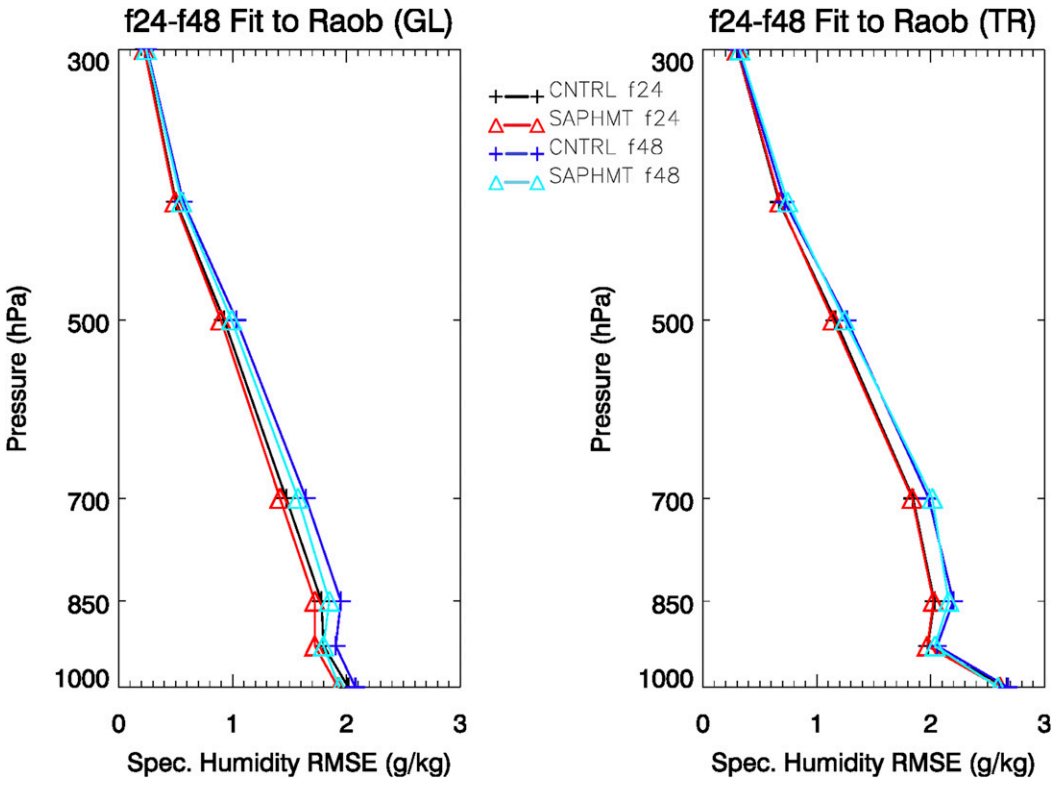

FIG. 13. Comparison of (left) specific humidity bias and (right) RMSE for CNTRL and SAPHMT 24- and 48-h forecasts verified against global radiosonde observations.

Verification of the 24- and 48-h forecasts was also performed against radiosonde observations for specific humidity, temperature, and wind speed since ECMWF analyses, though often used for verification, are not necessarily representative of the truth. The assessment contains the comparison to radiosondes accumulated globally throughout the forecast period (~100 000 radiosondes), as well as those just at the tropical latitudes from 20°S to 20°N (~20 000 radiosondes).

We show the specific humidity bias and RMSE from 1000 to 300 hPa, for both the CNTRL and SAPHMT experiment forecasts verified against global radiosondes (Fig. 13, left) and verified against only radiosondes in the tropics (Fig. 13, right). For the global comparison, the largest reduction (about 6%) in specific humidity RMSE when SAPHIR is assimilated occurs around 850 hPa at 48 h, but a reduction in forecast specific humidity RMSE is apparent from 1000 to 500 hPa for both forecast lead times. It should be noted that the radiosondes themselves are assimilated in the GDAS, thereby resulting in the retention of their history even when used in verifying short-term forecasts. Assessment of the specific humidity RMSE verified against only radiosonde data at tropical latitudes showed only a small improvement of around 2% at the surface for the 24-h forecast and mixed results at 48 h, where below 800 hPa there was 1%–3% improvement, but where a 3%–4% degradation was present above 500 hPa. Radiosonde humidity information is not trusted above 300 hPa, so the improvements shown in the comparison to ECMWF in Fig. 10 cannot be confirmed by radiosonde. The finding that the impact of assimilating SAPHIR on the humidity forecast is larger outside of the tropics, and at longer lead times, however, suggests that the information from SAPHIR is improving the forecast initial conditions and the subsequent transport of that moisture outside of the tropics.

Figure 14 shows the verifications of the temperature forecast at 24 and 48 h using radiosondes globally, as well as in the tropics only. The results suggest that SAPHIR is having a positive impact on the temperature RMSE globally, with about 1% improvement in the troposphere at 24 h, except around the tropopause region, and 1%–3% improvement at 48 h. In the tropics, there is little impact at 24 h, but a large reduction in the RMSE of temperature exists at 48 h (about 9% at 200 hPa) when assimilating SAPHIR. This could suggest that the assimilation of SAPHIR observations and the added information in upper-level humidity from the 183 ± 0.1 GHz band, as shown by the analysis and forecast improvements around 100 hPa, could be helping to

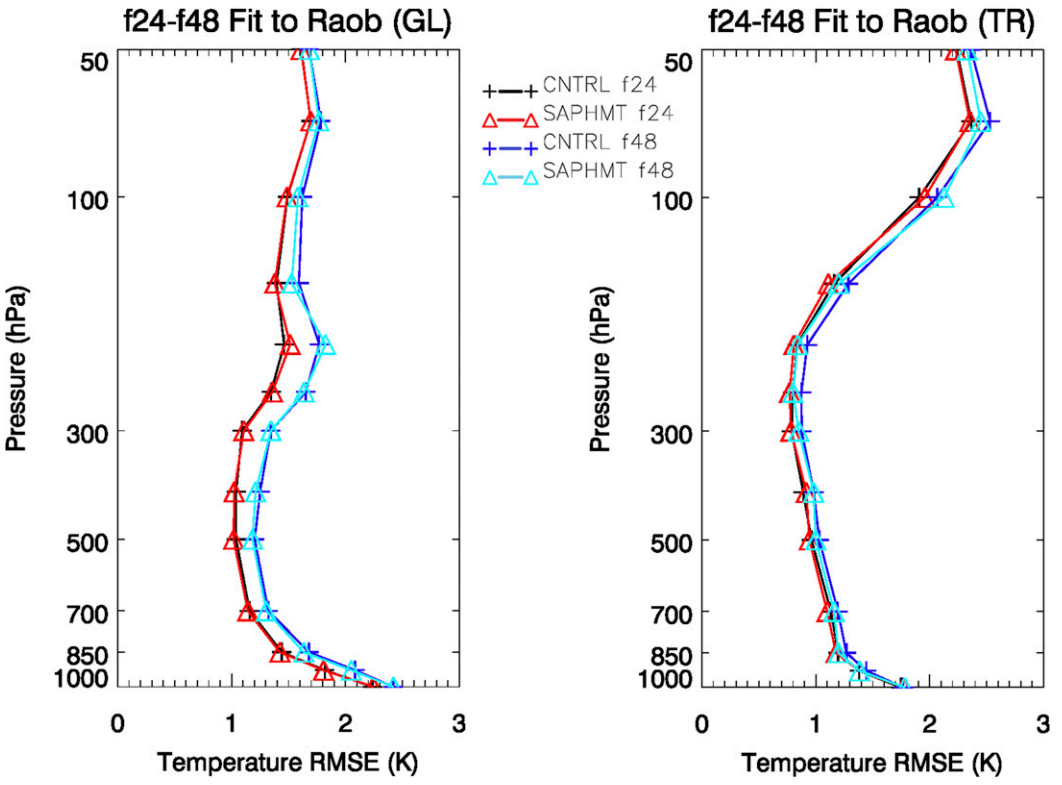

FIG. 14. As in Fig. 13, but for (left) temperature bias and (right) RMSE for forecasts verified against tropical radiosonde observations.

improve the temperature analysis through the moisture constraints in the background error covariance.

The impact on the forecast wind speed by the assimilation of SAPHIR was also assessed using radiosonde data as a reference. Globally, there is negligible impact on wind RMSE for the 24-h forecast but a more positive impact of around 4%–5% improvement at 150–200 hPa for the 48-h forecast (Fig. 15). The largest impact was seen in the tropics for the 48-h forecast, however, where the wind speed RMSE was reduced between 250 and 100 hPa by about 2%–7%, most likely because of differences in the mean analysis increment between the SAPHMT and CNTRL experiments for the meridional (V) wind component (not shown). It is possible that these small differences ($<0.5\,\mathrm{m\,s^{-1}}$) are driving changes in the forecast of the Hadley circulation strength and advection of the added moisture information from SAPHIR to the extratropics, resulting in the improvement seen in the global humidity forecasts in Fig. 13.

4. Conclusions

Observations from the SAPHIR instrument on the *Megha-Tropiques* have been successfully assimilated into the NOAA GDAS/GFS. QC methods were developed, including a GWP retrieval, to characterize the SAPHIR brightness temperatures in clear-sky conditions over ocean surfaces. The assessment of data quality showed small departures from simulation (<2 K) for the brightness temperatures of the six water vapor channels of SAPHIR after points affected by scattering from convective ice were removed, and guided specification for observation errors in the data assimilation system. Two experiments were run using the GDAS/GFS at T254 and T670 resolutions: the CNTRL run, which assimilates all observations currently assimilated operationally, and the SAPHMT experiment, which adds SAPHIR observations on top of the current observing system. The impact on GDAS analysis, when verified against ECMWF, showed a significant improvement of around 6% for upper-level humidity fields at 100 hPa, and generally positive or neutral impacts elsewhere over the atmospheric column after assimilating SAPHIR brightness temperatures, though some significant degradation (3%–5% increase in RMSE and standard deviation) in analysis humidity fields relative to ECMWF was seen at 850–700 hPa in the tropics. The added information content to the analysis and forecast also demonstrated an improvement in the assimilation of other similar water vapor sounding instruments; the

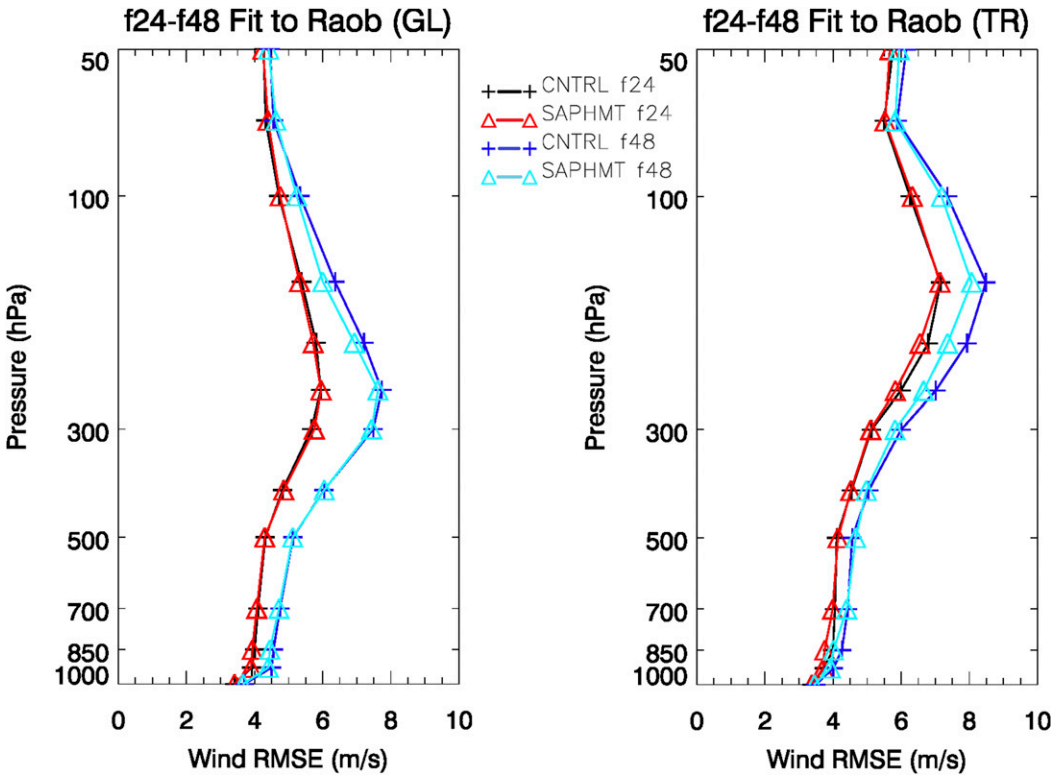

FIG. 15. As in Fig. 13, but for (left) wind bias and (right) RMSE forecasts verified against tropical radiosonde observations.

OmB statistics of 183-GHz channels from both *SNPP* ATMS and *F17* SSMIS improved when SAPHIR was assimilated in experiment analyses. For SSMIS, these improvements were significant for all 183-GHz channels globally and in the tropics, and for ATMS the improvements were significant globally for the two lowest-peaking 183-GHz channels and in the tropics for all 183-GHz channels except 183 ± 1.0 GHz. The assimilation of SAPHIR brightness temperatures additionally had a positive impact on GFS forecast fields of RH at 100 hPa until at least 72 h globally and in all regions examined (the tropics, Northern Hemisphere, and Southern Hemisphere) when verified against ECMWF analyses. This improvement at 100 hPa was most pronounced for short-term (24–72 h) forecasts, and in the Northern Hemisphere, where improvements were significant out past 144 h. Impacts elsewhere over the atmospheric column were generally neutral when analyzed over the global domain, though some significant degradation was seen in the short-term RH forecasts (24–48 and 24 h, respectively) at 150 and 200 hPa, which can be attributed to a degradation in RH RMSE in the tropics. Verification against radiosonde observations also confirmed the improvement in the humidity forecasts, showing a 4%–6% reduction in specific humidity RMSE from 1000 to 500 hPa at 24- and 48-h lead times, when assessed globally. Positive impact was also found through the 48-h forecast RMSE reduction of the upper-tropospheric temperature (9%) and wind fields (7%) in the tropics, though it should be noted that significance testing for the verification against radiosondes could not be performed for these experiments, and it is not meant to be implied that the results are significant in this case. The results do, however, suggest that the additional information from SAPHIR may be driving the improved forecast of the Hadley circulation and advection of moisture poleward in the upper troposphere.

The capability to assimilate SAPHIR observations was included in the July 2017 upgrade to NOAA's operational modeling suite, and the observations are being assimilated for monitoring in the operational system. It is expected that SAPHIR observations will be actively assimilated in the operational global model at NOAA with planned upgrades to the modeling suite in 2018. Future capabilities in assimilating observations from *Megha-Tropiques* SAPHIR will include observations over nonocean areas and in cloudy and precipitating conditions.

Acknowledgments. We would like to thank NOAA/NCEP/Environmental Modeling Center (EMC) along with the Joint Center for Satellite Data Assimilation Research to Operations Team for providing the data assimilation system, forecast data, observational datasets, and forecast verification datasets, along with assessment utilities. We would also like to thank Philippe Chambon and Météo-France for providing the *Megha-Tropiques* SAPHIR L1A2 data in BUFR format, and Rahul Mahajan of NOAA/NCEP for his assistance in generating a figure for this manuscript (and for being Rahul Mahajan).

REFERENCES

Andersson, E., and Coauthors, 2007: Analysis and forecast impact of the main humidity observing systems. *Quart. J. Roy. Meteor. Soc.*, **133**, 1473–1485, doi:10.1002/qj.112.

Bengtsson, L., and K. Hodges, 2005: On the impact of humidity observations in numerical weather prediction. *Tellus*, **57A**, 701–708, doi:10.3402/tellusa.v57i5.14734.

Boukabara, S.-A., K. Garrett, and W. Chen, 2010: Global coverage of total precipitable water using a microwave variational algorithm. *IEEE Trans. Geosci. Remote Sens.*, **48**, 3608–3621, doi:10.1109/TGRS.2010.2048035.

Brogniez, H., and Coauthors, 2016: A review of sources of systematic errors and uncertainties in observations and simulations at 183 GHz. *Atmos. Meas. Tech.*, **9**, 2207–2221, doi:10.5194/amt-9-2207-2016.

Chambon, P., L.-F. Meunier, F. Guillaume, J.-M. Piriou, R. Roca, and J.-F. Mahfouf, 2015: Investigating the impact of the water-vapour sounding observations from SAPHIR on board Megha-Tropiques for the ARPEGE global model. *Quart. J. Roy. Meteor. Soc.*, **141**, 1769–1779, doi:10.1002/qj.2478.

English, S. J., R. J. Renshaw, P. C. Dibben, A. J. Smith, P. J. Rayer, C. Poulsen, F. W. Saunders, and J. R. Eyre, 2000: A comparison of the impact of TOVS and ATOVS satellite sounding data on the accuracy of numerical weather forecasts. *Quart. J. Roy. Meteor. Soc.*, **126**, 2911–2931, doi:10.1002/qj.49712656915.

Eymard, L., and Coauthors, 2001: The SAPHIR humidity sounder. *Proc. Second Megha-Tropiques Scientific Workshop*, Paris, France, Indian Space Research Organisation–Centre National d'Etudes Spatiales. [Available online at http://meghatropiques.ipsl.polytechnique.fr/dmdocuments/proc_s3p02.pdf.]

Geer, A. J., F. Boardo, N. Bormann, and S. English, 2014: All-sky assimilation of microwave humidity sounders. ECMWF Tech. Memo. 741, 57 pp. [Available online at https://www.ecmwf.int/sites/default/files/elibrary/2014/9507-all-sky-assimilation-microwave-humidity-sounders.pdf.]

Han, Y., P. van Delst, Q. Liu, F. Weng, B. Yan, R. Treadon, and J. Derber, 2006: JCSDA Community Radiative Transfer Model (CRTM) - version 1. NOAA Tech. Rep. NESDIS 122, 31 pp. [Available online at https://docs.lib.noaa.gov/noaa_documents/NESDIS/TR_NESDIS/TR_NESDIS_122.pdf.]

McClung, T., 2014: Technical implementation notice 14-46. NOAA/NWS. [Available online at http://www.nws.noaa.gov/os/notification/tin14-46gfs_cca.htm.]

McNally, A. P., J. C. Derber, W. Wu, and B. B. Katz, 2000: The use of TOVS level-1b radiances in the NCEP SSI analysis system. *Quart. J. Roy. Meteor. Soc.*, **126**, 689–724, doi:10.1002/qj.49712656315.

Seemann, S. W., J. Li, L. E. Gumley, K. I. Strabala, and W. P. Menzel, 2003: Operational retrieval of atmospheric temperature, moisture, and ozone from MODIS infrared radiances. *Applications with Weather Satellites*, W. P. Menzel et al., Eds., International Society for Optics and Photonics (SPIE Proceedings, Vol. 4895), 168–176, doi:10.1117/12.466686.

Singh, R., S. P. Ojha, C. M. Kishtawal, and P. K. Pal, 2013: Quality assessment and assimilation of Megha-Tropiques SAPHIR radiances into WRF assimilation system. *J. Geophys. Res. Atmos.*, **118**, 6957–6969, doi:10.1002/jgrd.50502.

Sun, J., 1993: Effects of vertical distribution of water vapor and temperature on total column water vapor retrieval error. *J. Geophys. Res.*, **98**, 7069–7079, doi:10.1029/93JC00010.

Wang, X., D. Parrish, D. Kleist, and J. Whitaker, 2013: GSI 3DVar-based ensemble-variational hybrid data assimilation for NCEP Global Forecast System: Single-resolution experiments. *Mon. Wea. Rev.*, **141**, 4098–4117, doi:10.1175/MWR-D-12-00141.1.

Zhu, Y., J. Derber, A. Collard, D. Dee, R. Treadon, G. Gayno, and J. A. Jung, 2014: Enhanced radiance bias correction in the National Centers for Environmental Prediction's Gridpoint Statistical Interpolation data assimilation system. *Quart. J. Roy. Meteor. Soc.*, **140**, 1479–1492, doi:10.1002/qj.2233.